UC Irvine
UC Irvine Previously Published Works

Title

High speed three-dimensional endoscopic OCT using MEMS technology

Permalink

ISBN

9780819465795

Authors

Chen, Z
Jung, W
Ahn, YC
et al.

Publication Date

2007-04-30

DOI

10.1117/12.713950

Copyright Information

Peer reviewed

High speed three-dimensional endoscopic OCT using MEMS technology

Zhongping Chen[1,2], Woonggyu Jung[1,2], Yeh-Chan Ahn[1], Ali Sepehr[1,3], William B. Armstrong[3], Matt Brenner[1,4], Daniel T. McCormick[5,6], Norman C. Tien[7]

[1]Beckman Laser Institute, University of California, Irvine
[2]Department of Biomedical Engineering, University of California, Irvine
[3]Department of Otolaryngology-Head and Neck Surgery, University of California, Irvine
[4]Department of Pulmonary Medicine, University of California, Irvine
[5]Berkeley Sensor and Actuator Center
[6]Department of Electrical Engineering and Computer Science, University of California, Berkeley
[7]Department of Electrical and Computer Engineering, Case Western Reserve University, Cleveland

ABSTRACT

We present a three-dimensional (3-D) endoscopic optical coherence tomography (OCT) system using a dual axis scanning mirror. The MEMS device employed in this study utilized a 1.2 mm mirror and exhibited x and y-axis resonant frequencies greater than 1 kHz. The developed probe was packaged and integrated with an OCT system which has a scan rate of 3~8 frames/s. Preliminary in vivo and in vitro 3-D OCT images of biological tissue, such as human finger, vocal cord, rabbit trachea, were visualized to verify the achieved performance of the device.

Keywords: Endoscopic Optical CoherenceTomography (OCT), MEMS Technology, 3D Imaging

INTRODUCTION

Optical coherence tomography (OCT) is a noninvasive imaging modality that permits high resolution, cross-sectional imaging of scattering media in real time [1]. OCT is based on optical coherence reflectometry which is analogous to ultrasound imaging but utilizes a broadband light source instead of sound waves to measure the intensity of back-reflection as function of depth in the sample. Following the initial clinical use of OCT in ophthalmology, OCT has subsequently been applied to visualize various biological tissue, skin, blood vessels and the oral cavity [2-5]. However, for many clinical applications the development of miniaturized optical beam delivery systems is required. For example, endoscopic probes are needed for imaging of internal organs because OCT has a limited penetration depth of 2-3 mm into complex tissue. For this purpose, various OCT endoscopes have been developed in which linear as well as rotational scanning is generated [2,5-7]. Several research groups have demonstrated the potential capabilities of OCT imaging using endoscopes in internal tissues, such as airway and gastrointestinal tracts. The most common OCT endoscope designs require the entire distal probe apparatus to be mechanically moved from the proximal end for scanning usually through cable transduction methods. In order to eliminate this drawback, Pan et al. and Zara et. al. developed a one dimensional scanning (1-D) microelectromechanical system (MEMS) mirror for endoscopic OCT [8,9]. To date, most endoscopic OCT has been focused on two dimensional imaging, but 3-D imaging is more ideal for many clinical applications because 3-D imaging can provide clinicians not only additional visualization but also fully spatially realized diagnostic information. Recently, many three- dimensional (3-D) OCT systems have been reported due to advances in OCT technology enabling high speed imaging and acquisition, such as Fourier-domain (FD) and spectral-domain (SD) OCT systems [10-12]. Conventional scanning methods, including rotating and linear scanning (push-pull motion) mechanisms do allow 3-D endoscopic OCT imaging but are not ideal due to complex positioning, hysteresis, requirements for cable movement along the entire length of the endoscopic probe, and consequent limitations in imaging speed.

In this letter, we demonstrate a 3-D endoscopic OCT system using a MEMS based 2 axis scanning mirror [13]. Because our probe employed MEMS technology, it has many advantages over prior designs, including rapid scanning, small size, high reliability, and flexibility in scanning pattern capabilities. This 3-D OCT system high speed 2-D scanning provides the potential to deliver real time high resolution diagnostic information to physicians as well as rapidly identify areas of interest during endoscopy. Here, we describe the design and structure of the 2 axis scanning mirror and verify the ability of the 3-D high speed OCT system using a developed probe.

MEMS DEVICES & ENDOSCOPIC PROBE

A generalized schematic of the 3-D endoscopic OCT probe employing a MEMS mirror is presented in Fig. 1A. The probe is consists of a pigtailed GRIN lens and MEMS mirror which were aligned and assembled in a package which provides optical alignment, electrical connections, mechanical protection and an optical window for imaging. Fig. 1B is an image of a two axis MEMS mirror.
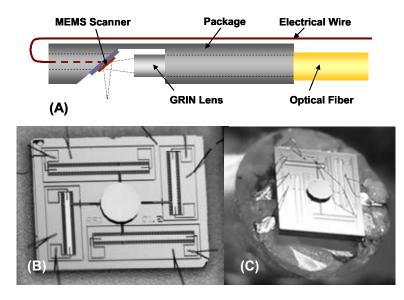

FIG. 1. (A) Schematic of completed 3-D endoscopic MEMS probe; (B) A stereo microscope image of a two axis MEMS mirror; (C) An optical micrograph of a scanner with attached mirror with wirebond connections to an acrylic package.

The MEMS scanning actuator employed in this work is a monolithic, single crystal silicon (SCS), 2-dimensional, gimbal-less, vertical comb-driven structure [14,15]. The devices were designed and realized in a self-aligned DRIE fabrication process utilizing a silicon on insulator (SOI) wafer. The MEMS scanners were diced during the fabrication process, eliminating the possibility of damage and contamination from a scribing or wafer sawing step. The mirrors were fabricated in a separate SOI process and later bonded to the actuator allowing the actuator and mirror to be independently optimized. The mirror apertures were metalized low-inertia SCS structures using a thinned mirror plate (2-5 µm), thick stiffening trusses (~25 µm) and a tall standoff pedestal (~120 µm). The device employed in this particular study had a 1.2 mm diameter mirror and exhibited x- and y-axis resonant frequencies of 1.8 kHz and 2.4 kHz, respectively. The scan angle of each axis was approximately 20° (optical). The maximum drive voltage mirror in this experiment was 100 V, and the device was driven such that a stepped linear at the tissue plane was achieved. During imaging the mirror is directed to point to a specific location and is held stationary during acquisition of that voxel's back-reflected signal, the mirror is then stepped to the next location. Constant velocity or any arbitrary scan patterns may also be selected. While characterizing the probe, the accuracy as well as precision of the scan was verified employing a position sensitive diode (PSD) and optical feedback system. The amplifier driving the devices delivered a maximum voltage of 150 V during drive transients; however, the electrostatic comb-structures required very small current levels to operate and the amplifier incorporated several protection mechanisms.

A photograph of the packaged endoscopic OCT probe with MEMS mirror is shown in Fig. 2. Four generations of 3-D endoscopic probes have been fabricated and tested. The smallest probes realized to date have an outer diameter of 3.9 mm (Fig. 2A). These probes were fabricated from a machined acrylic rod; concentric holes sharing the same center point were drilled through the central axis, following a common guide hole, in order to allow accurate and precise alignment of the optical components. Six small (300 μm diameter) holes were then drilled from the distal end of the probe in order to provide electrical connections to the mirror. A 45° platform was then machined to serve as a support for the mirror die; sufficient material remained on the tube walls to maintain mechanical rigidity and structural integrity (Fig. 1C). Wires with a diameter of 200 μm were then passed through the access holes and secured in place with epoxy; the surface of the wires were then planarized and served as bonding pads. The tail of the wires were bent back and run through a channel along the bottom of the probe. Next a GRIN lens with a pig-tailed optical fiber was inserted into the package and temporarily held in place while the MEMS mirror was positioned on the machined platform. The alignment of the components was completed utilizing a stereoscope and a visible laser coupled into the GRIN lens. The MEMS device was then fixed in place, and the wirebond connections were made between the MEMS die and the package.
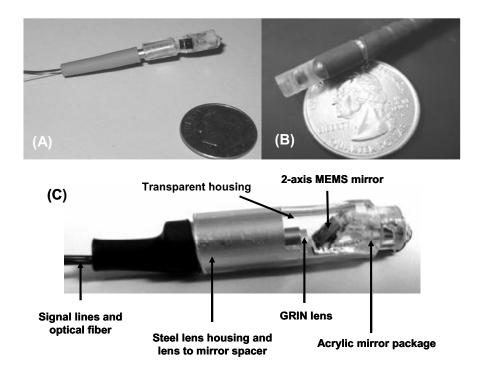

FIG. 2. Photograph of the completed probes. (A) The 1st generation probe, 3.9 mm, next to a US dime. (B) 4th generation probe, 5.0 mm, compared to a US quarter. (C) Magnified photograph of 2nd generation probes. The steel lens housing provides rigid as well as proper alignment with and spacing to the MEMS device; outer diameter of the probe is 4.9 mm.

In the 2nd and 3rd generation of the endoscopic probes, machined steel and plastic tubes provided rigidity and alignment of the GRIN lens to the MEMS mirror; in addition, this piece contained a spacer to insure proper working distance between the lens and mirror surface. A machined acrylic mount positioned the mirror 45° angle and provided access holes for the signal wires. The mirror was then attached to the mount and wirebonds connected the silicon to the signal leads. The lens alignment pieces and mirror mount were inserted into a transparent tube from opposite ends. Epoxy and heat shrink tubing were used to seal and protect the probe. The 2nd and 3rd generation of probes were 4.9 mm and 5.5 mm in diameter, respectively. With the visible and 1310 nm source, alignment and operation is verified; after the desired focal point location was achieved, the GRIN lens was then permanently fixed in the package. The specific GRIN lens (ϕ 1. 4 mm) utilized in this study had a 6.6 mm working distance and approximately 20 μm spot size at the focal plane.

OCT SYSTEMS

The packaged endoscopic probe was integrated with fiber based OCT systems; time domain (TD), Fourier domain (FD), and spectral domain (SD) OCT systems (Fig. 3A.).
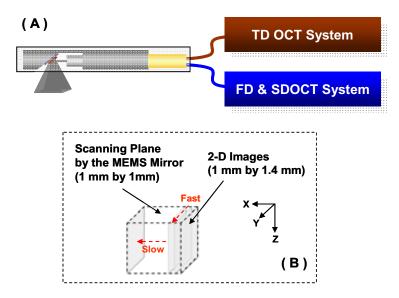

FIG. 3. (A) Developed endoscopic probes were combined with TD, FD and SD OCT systems. (B) The scanning methodology of the MEMS mirror and the generation of a volume image by stacking of images is shown in the TD OCT system. X, Y axis indicates slow and fast axis scanning by MEMS mirror and Z axis indicates depth scanning by RSOD.

The TD OCT system employed a low-coherence length light source that delivered an output power of 10 mW at a central wavelength of 1310 nm with a bandwidth of 80 nm, providing 10 μm axial resolution. A visible aiming beam (633 nm) was utilized to locate the exact position and path on the sample, and both light sources were coupled into a fiber-based Michelson interferometer. In the reference arm, a rapid-scanning optical delay line (RSOD) was used that employed a grating to control the phase and group delays separately so that no phase modulation was introduced when the group delay was scanned[16]. The phase modulation was generated through an electro-optic phase modulator that produced a stable carrier frequency. The axial line scanning rate was 500 Hz, and the modulation frequency was 500 kHz. In the sampling arm, the previously described MEMS scanner was employed to provide sample scanning; the MEMS device was controlled by custom electronics interfaced to the OCT data acquisition system. A 2-D cross-sectional image was acquired by a lateral scan (A-scan) by one axis of the MEMS scanner and depth scanning (B-scan) via the RSOD. In an analogous manner with 2-D imaging, for 3-D OCT imaging, a 2-D image was first achieved by combination of one axis scanning of the MEMS scanner sequentially after each depth scan of the RSOD. Then, the second axis of the MEMS mirror moved one "step" to the next position and another 2-D image was obtained. This sequence was continuously repeated until the scanning area specified by the operator was completed. In Fig. 3B, the dashed box provides a schematic summary of the 3-D scanning methodology. The reflected beams from the sample and reference arms were recombined in the interferometer and the detected optical interference fringes signals from the photodetector were filtered at the carrier frequency. The resulting signals were automatically displayed as 2-D images in real-time, saved to the computer, accumulated, and visualized as a 3-D image after post-image processing, such as iso-surface extraction, filtering, thresholding, pseudo-coloring, animation and region selection.

In the FD OCT system, a swept laser source at 1.31 μm with a FWHM bandwidth of 85 nm and output power of 5 mW was utilized. The source was driven by a 2 kHz sinusoidal signal coupled into a fiber-based Michelson interferometer. In the reference arm, an electro optic (EO) phase modulator was used to generate a stable carrier frequency of 2 MHz for elimination of the mirror image and low frequency noise [10]. To match the dispersion caused by the EO phase modulator, an optical setup similar to a RSOD line with a stationary mirror was adopted which can compensate the second order group velocity dispersion. The reference power was attenuated by an adjustable neutral density attenuator for maximum sensitivity. Approximately, 5% of the laser output was split and propagated through a 100 GHz fiber Fabry-Perot (FFP) interferometer to generate comb signals for dynamic calibration of the swept wavenumber function

that is essential for rigorous conversion from time to wavenumber space. Light returned from the sampling arm and reference arm recombined into a fiber-based Michelson interferometer and a generated interference signal was directed to photodetectors. In the SD OCT system, low-coherence light having a center wavelength of 1310 nm with a full width half maximum bandwidth 95 nm was coupled into a fiber-based Michelson interferometer. Back-reflected lights from the reference and sample arms were guided into a spectrometer. The dispersed spectrum was sampled by a 1×1024 InGaAs detector array at 7.7 kHz. The wavelength range on the array was 130 nm, corresponding to a spectral resolution of 0.13 nm. When the optical paths at the both arms matched, an interference pattern was generated on the detector array. As in the TD OCT system, endoscopic probes were also used in the sampling arm of both the FD and SD systems. Since the FD and SD systems do not need mechanical scanning along the depth axis, a 2-D image was generated by acquiring a depth modulated signal sequentially while the fast axis of the MEMS mirror scanned. Then, the slow axis of the MEMS mirror moved to the next position and 2-D images were reconstructed to 3-D images.

CLINICAL STUDIES

For the clinical studies, the developed endoscopic OCT probes were integrated with conventional endoscopes. The diameter of the endoscopic OCT probe used in these studies was around 5 mm, which is too large to fit into the biopsy channel of a conventional flexible bronchoscope. Thus, the endoscopic OCT probes were attached to a outside of the endoscope as shown in Fig.4A,B. In our study, a flexible fiberoptic bronchoscope and rigid telescope were used in order to guide the path of OCT probe. Fig. 4A shows that the probe is tethered to the flexible and rigid endoscope. With the flexible fiberoptic bronchoscope, a string loop methodology was utilized to tether the MEMS probe. Dental floss was passed down the working channel of the bronchoscope to create a loop at the distal end of the bronchoscope. The MEMS probe was passed through the loop, and the loop tightened from the proximal end to hold the probe in place. The bronchoscope with the tethered MEMS probe was then passed with direct visualization to the sites of interest. The probe could be manipulated by loosening the tension on the loop as needed (Fig. 4A.) The OCT was also coupled to a rigid endoscope for its application to the upper airway of human patients in the operating room (Fig. 4B.). The patient was taken to the operating room, placed on the operating table under general anesthesia and intubated. The MEMS probe was covered by an optically transparent PTFE sheath, and the OCT probe was attached directly to a 0 degree rigid endoscope using 0.25" adhesive tape that is specifically used for biological applications. The distal tip of the OCT probe was approximately 3 cm in front of the distal tip of the endoscope. Furthermore, the probe was oriented such that the OCT beam crossed the field of view of the endoscope. The axial and rotational orientation allowed placement of the OCT probe on the desired tissue under direct endoscopic visualization. A light source and camera were attached to the rigid endoscope. Fig. 4C shows the video captured image by endoscope camera which identified the location and guided the movement of the MEMS probe in the airway. In our experiment, the light source at 10-25% was used to see visible light from the MEMS probe (dotted line in Fig. 4C). For the optical biopsy, a suspension laryngoscope was inserted and fixed in place. Under direct endoscopic visualization, OCT images of the laryngeal surface of the vocal cords were obtained. In order to obtain high quality images, care was taken to minimize any motion on the part of the patient and technician for the duration of imaging (approximately 15 seconds).
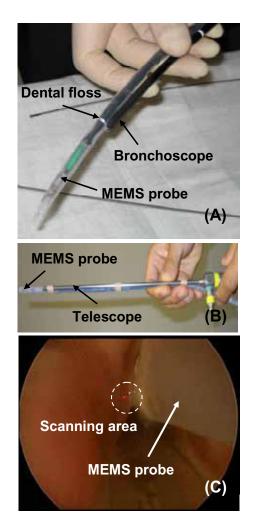

FIG. 4. MEMS probe tethered to the flexible fiberoptic bronchoscope (A) and rigid telescope (B) for visualization and directed passage through airways. (C) Images of MEMS probe in human upper airways. The endoscope camera guides location and movement of MEMS probe in the upper airway.

RESULTS

Fig. 5(A-C) presents 3-D images acquired by the TD OCT system at a rate of 3 frames/s. The size of volume image was 1 mm × 1 mm × 1.4 mm. In the 3-D images, thresholding was used to visualize only biological tissue structures of interest. Fig. 5A shows a cross sectional 3-D image of rabbit trachea. In the image, tissue structures, such as the epithelum, glands, and cartilage, were clearly visualized. To further evaluate the feasibility of the 3-D MEMS probe for clinic application, both normal and cancerous regions of tissue from a hamster cheek pouch were imaged (shown in Fig. 5B and 5C). In the OCT image of normal tissue (Fig. 5B), the layered structures are clearly visible with vivid border lines, including the basement membrane. The observation of the basement membrane as a superficial layer is particularly meaningful for clinicians to detect and diagnose early cancer. This membrane provides basic information regarding identification and diagnosis of pre-cancer, such as dysplasia [11]. In contrast to the image of normal tissue, layered structures are not visible and the base membrane is not distinguished clearly in the cancerous tissue as presented in Fig. 5C. Fig. 5(D-F) present OCT images which were obtained utilizing the FD OCT system at a rate of 8 frames/s. The size of volume image was 1 mm × 1 mm × 2 mm. Similar to Fig. 5A, many important features of rabbit trachea, the epithelum, glands, and cartilage, are visualized as shown in Fig. 5D. Fig. 5E and 5F present *in vivo* 3-D OCT image of a finger at 180° camera perspectives. In both images, tissue structures such as epitherial layer, epidermal layer, sweat ducts are clearly distinguished. These results demonstrate that 3-D endoscopic OCT is a promising tool to visualize useful morphology at any location using post-image processing.
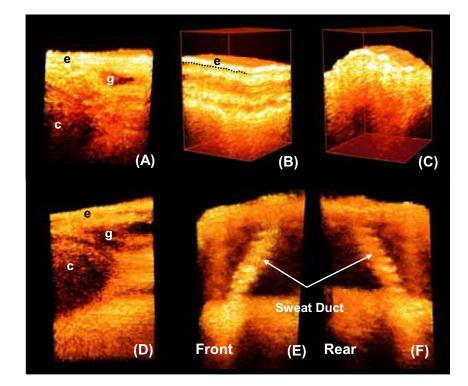

FIG. 5. (A-C) 3-D OCT images obtained by TD OCT system: Images were acquired at a rate of 3 frames/s and have a size of 1 mm × 1 mm × 1.4 mm. (A) Image of rabbit trachea. Important tracheal structures such as the epithelium (e), glands (g), and cartilage (c) are clearly visible. (B) Image of normal hamster cheek pouch. Vivid layered structures including the epithelium (e) are visualized. The dotted line indicates the base membrane. (C) OCT image of cancerous hamster cheek pouch.; (D-F) 3-D OCT images obtained by FD OCT system: Images were achieved at a rate of 8 frames/s and visualized as volume with 1 mm × 1 mm × 2 mm 1 mm. (D) Image of rabbit trachea. Similar to Fig. 5D, tissue structures, such as the epithelium (e), glands (g), and cartilage (c), are clearly visualized. (E,F) In vivo images of a finger at front and rear. The arrows indicate the sweat ducts.
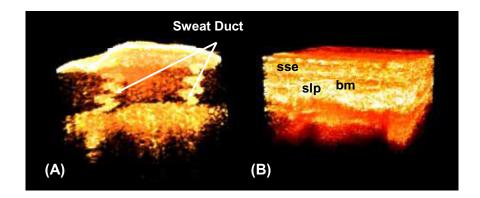
FIG. 6. In vivo 3-D OCT images obtained by SD OCT system: Images were acquired at a rate of 8 frames/s and have a size of 1 mm × 1 mm × 1.4 mm. (A) In vivo images of a finger; the arrows indicate the sweat ducts which are visualized as spiral shaped. (B) True vocal cord of human. Important structures such as the stratified squamous epithelium (sse), basement membra (bm), and superficial lamina propria (slp) are clearly visible.

In vivo 3-D images of a human subject are shown in Fig. 6. This image was acquired employing the SD OCT system at a rate of 8 frames/s. The image of tissue volume was 1 mm × 1 mm × 1.4 mm. Resembling Fig. 5E,F clear tissue structures, such as epithelial layer, epidermal layer, sweat ducts were visualized. The image has been thresholded to emphasize the spiral structure of the sweat ducts. *In vivo* 3-D images were also obtained of the laryngeal surface of the epiglottis and false and true vocal cords under endoscopic visualization. One of the volume images is presented in Fig. 6B. Detailed structures, such as the stratified squamous epithelium (sse), basement membra (bm), and superficial lamina propria (slp), are clearly visible. The optical biopsy of the vocal cords using 3D-OCT is of particular importance given the delicate nature of the vocal cord mucosa. If there is a lesion on the vocal cords, currently, the only way to differentiate benign from malignant is to perform a biopsy. This biopsy can damage the mechanical characteristics of the cords and lead to alteration of the mucosal wave during phonation, leading to a change in voice. Also, currently to ensure adequate resection of malignant lesions, a wider margin is taken which leads to greater than necessary voice changes. With an optical biopsy one could avoid damage in benign lesions altogether. By better defining the borders of malignant lesions, one could minimize the morbidity of the resection by doing a more limited and exact resection.

CONCLUSION

In summary, we have developed a 3-D endoscopic OCT system employing a 2-axis MEMS scanning probe and have demonstrated its potential as a real-time tool for optical biopsy. MEMS mirrors actuated by electrostatic comb-drives were incorporated with pigtailed GRIN lenses and packaged. The final 3-D endoscopic probes were integrated with fiber-based OCT systems and tested employing conventional endoscopes. Biological tissue from a human, rabbit and hamster were imaged; the resulting volume images provided morphological details, such as visualization of the epithelium, mucosa, and submucosa. As neither the speed limits nor the optical resolution of our MEMS devices have been reached, we will continue to develop faster imaging systems with high resolution capabilities. We are also continuing to work with physicians and clinicians to optimize the probes for use in a variety of applications.

ACKNOWLEDGMENTS

REFERENCES

1. D. Huang, E.A. Swanson, C. P. Lin, J. S. Schuman, W. G. Stinson, W. Chang, M. R. Hee, T. Flotte, K. Gregory, C. A. Puliafito, J. G. Fujimoto, Science **254**, 1178 (1991).
2. G. J. Tearney, M. E. Brenzinski, B. E. Bouma, S. A. Boppart, C. Pitris, J. F. Southern, J. G. Fujimoto, Science **276**, 2037 (1997).
3. M. R. Hee, J. A. Izatt, E. A. Swanson, D. Huang, C. P. Lin, J. S. Schuman, C. A. Puliafito, J. G. Fujimoto, Arch. Opthal. **113**, 326 (1995).
4. W. Jung, J. Zhang, J. Chung, P. W. Smith, M. Brenner, J. S. Nelson, Z. Chen, IEEE JSTQE., 11, **811**, 2005.
5. A. M. Rollins, R. Ung-arunyawee, A. Chak, R. C. K. Wong, K. Kobayashi, M. V. Sivak, J. A. Izatt, Opt. Lett. **24**, 1358 (1999).
6. B. E. Bouma and G. J. Tearney, Opt. Lett. **24**, 531 (1999).
7. Y. Wang, M. Bachman, G.. P. Li, S. Guo, B. J. F. Wong, Z. Chen, Opt. Lett. **30**, 53 (2005).
8. Y. Pan, H. Xie, G. K. Fedder, Opt. Lett. **26**, 1966 (2001).
9. J. M. Zara, S. Yazdanfar, K. D. Rao, J. A. Izatt, S. W. Smith, Opt. Lett. **28**, 628 (2003).
10. J. Zhang, J. S. Nelson, Z. Chen, Opt. Lett. **30**, 147 (2005).
11. S. H. Yun, G. J. Tearney, J. F. de Boer, N. Iftimia, B. E. Bouma, Opt.Exp. **11**, 2953 (2003)
12. S. Yun, G. Tearney, B. Bouma, B. Park, and J. F. de Boer, Opt. Exp. **11**, 3598
13. W. Jung, D. T. McCormick, J. Zhang, L. Wang, N. C. Tien, Z. Chen, Appl. Phys. Lett. **88**, 163901 (2006)
14. V. Milanović, IEEE/ASME J. MEMS. **13**, 19, (2004).
15. V. Milanović, D. T. McCormick, G. Matus, IEEE J. STQE., **10**, 462 (2004).
16. G. J. Tearney, B. E. Bouma, F. G.. Fujimoto, Opt. Lett. **22**, 1811 (1997).